Journal of Applied Electrochemistry (2006) 36:871–882
DOI 10.1007/s10800-005-9098-3

Electrodeposition of FeCoNiCu nanowires

Q. HUANG, D. DAVIS and E.J. PODLAHA*
Mary A. and Gordon Cain Department of Chemical Engineering, Louisiana State University, Baton Rouge, LA 70803, USA
*(*author for correspondence, e-mail: podlaha@lsu.edu)*

Received 1 May 2004; accepted in revised form 14 November 2005

Key words: Co-rich alloys, electrodeposition, nanowires, Magnetic multilayers

Abstract

Electrodeposition of FeCoNiCu/Cu nanometric, compositionally modulated alloy nanowires is presented. Pure Cu nanowires and Co-rich FeCoNiCu alloy nanowires were deposited from a single electrolyte. A double potential pulse scheme was used for multilayer deposition and significant anodic dissolution was observed during the low potential pulse. Galvanostatic triple pulses with a relaxation period were developed to minimize the local pH rise inside the nanopores during fabrication of the layered FeCoNiCu/Cu nanowires.

1. Introduction

Arrays of nanowires have potential applications in perpendicular ultra-high density data storage [1–4], and as chemical and bio-sensors [5–9]. For enhanced sensing applications the nanowire is composed of a multilayer structure with alternating ferromagnetic and nonmagnetic layers. Current perpendicular to the plane (CPP) of the multilayers results in giant magnetoresistance (GMR), a decrease in the nanowire resistance in an applied magnetic field, that can even surpass thin film multilayered electrodeposits as demonstrated by the large GMR values observed experimentally [10–12] and theoretically [13–14].

In current-in-plane, CIP–GMR, the characteristic scaling length is the electron mean-free path, which is a few nanometers. In contrast, for the CPP–GMR configuration, the critical length scale is the spin diffusion length, which is generally larger than 10 nm [15–16], and thus larger multilayer sizes can be tolerated. Therefore, the CPP–GMR design is easier to control for the electrodeposition process as it is beyond the nucleation characteristic size. For example, GMR has been observed in multilayer nanowires with a layer size of 12 nm NiFe/4 nm Cu [17] and 5 nm Co/8 nm Cu [18], larger than typical thin film multilayers.

In addition to the advantages of high deposition rate and cost effectiveness, electrodeposition is a superior method for deposition into curved and recessed areas, where nanowire fabrication is a case-in-point. Template electrodeposition of nanowires involves the use of a nonconductive, nanometric porous substrate. After the deposit fills up the pores, the nanowires are released from the template by dissolving it in an appropriate solution. Several types of templates have been used: anodic aluminum oxide (AAO), polycarbonate and diblock copolymer membranes. The AAO membrane is prepared by anodization of aluminum foil in sulfuric acid solutions, resulting in well-ordered pores in a hexagonal configuration [19–20]. In contrast, the polycarbonate membranes are prepared with a nuclear track etch process [21–23], and the pore size can be much smaller than the AAO. Another method for template preparation is the self-assembly of diblock copolymers, such as poly-styrene–methyl methacrylate (PS-r–MMA) where MMA is selectively removed resulting in a hexagonally packed porous template [24–25].

A variety of metals, unlayered alloys and multilayered structures have been electrodeposited into templates to form nanowires. Single metal nanowires of Co [4, 26–29], Fe [4, 29–30] and Ni [31], and unlayered alloys of CoNi [32] and CoFe [33–34] have been studied, primarily for the preferred perpendicular magnetic anisotropy along the wire length and enhancement in coercivity. Nanowires of multilayers have been investigated for a few systems. Piraux et al. [35] studied the CPP–GMR of Co/Cu multilayer nanowires with a GMR value about 15% found at room temperature. The GMR at 4 K was found to be almost the same as its room temperature value, which has also been observed by other authors [15, 17, 36]. Blondel et al. [36] and Schwarzacher et al. [12] studied CoNi/Cu nanowires, and have reported one of the highest electrodeposited GMR at room temperature, 55%. NiFe/Cu multilayer nanowires were fabricated by Dubois et al. [17] and were found to exhibit 20% at ambient temperature and

about 80% at 4 K. This system was also studied by Blondel et al. [36] with a lower GMR observed.

Despite the numerous research efforts on nanowire deposition for different systems, few studies have been carried out on alloys and multilayers for alloy systems containing more than two elements. In our previous study, nanometric FeCoNiCu/Cu multilayers were fabricated for GMR [37–38]. In this paper, electrodeposition conditions are explored for fabricating FeCoNiCu alloy and multilayer nanowires. To the best of the authors' knowledge this is the first demonstration of FeCoNiCu nanowires or FeCoNiCu/Cu multilayered nanowires.

Table 1. Composition of different solutions for nanowire plating

Constituent	Bath A	Bath B
$FeSO_4 \cdot 7H_2O$/mol l^{-1}	0.008	0.1
$CoSO_4 \cdot 6H_2O$/mol l^{-1}	0.050	0.5
$NiSO_4 \cdot 6H_2O$/mol l^{-1}	0.057	–
$Ni(SO_3NH_2)_2 \cdot 6H_2O$/mol l^{-1}	–	0.5
$CuSO_4 \cdot 5H_2O$/mol l^{-1}	0.001	0.003, 0.03, 0.01
$NaKC_4H_4O_6 \cdot 4H_2O$/mol l^{-1}	0.027	0.1
Sulfamic Acid/mol l^{-1}	0.0103	0
Sodium Saccharin/mol l^{-1}	0.0041	0
Triton X-100 (g l^{-1})	0.6	0.6
pH	2.5	Natural (3.1)

2. Experimental

Two electrolytes, listed in Table 1, were investigated for nanowire plating. Bath A is a dilute electrolyte, which was previously used in multilayer thin film plating [37]. Bath B is a more concentrated electrolyte than Bath A, chosen in order to compensate for the longer diffusion distance in AAO membrane templates. The concentration of iron-group metal ions is higher than Cu(II) ions, in order to plate the magnetic layer containing a minimum of Cu. Nickel sulfamate is used in Bath B, instead of sulfate, adopted from MEMS micro-recess plating, where low-stress deposits are critical [39].

A gold rotating disk electrode (RDE), platinum mesh anode and a SCE (saturated calomel electrode) were used to characterize the solutions. Polarization curves were carried out with a Pine Instruments bi-potentiostat,

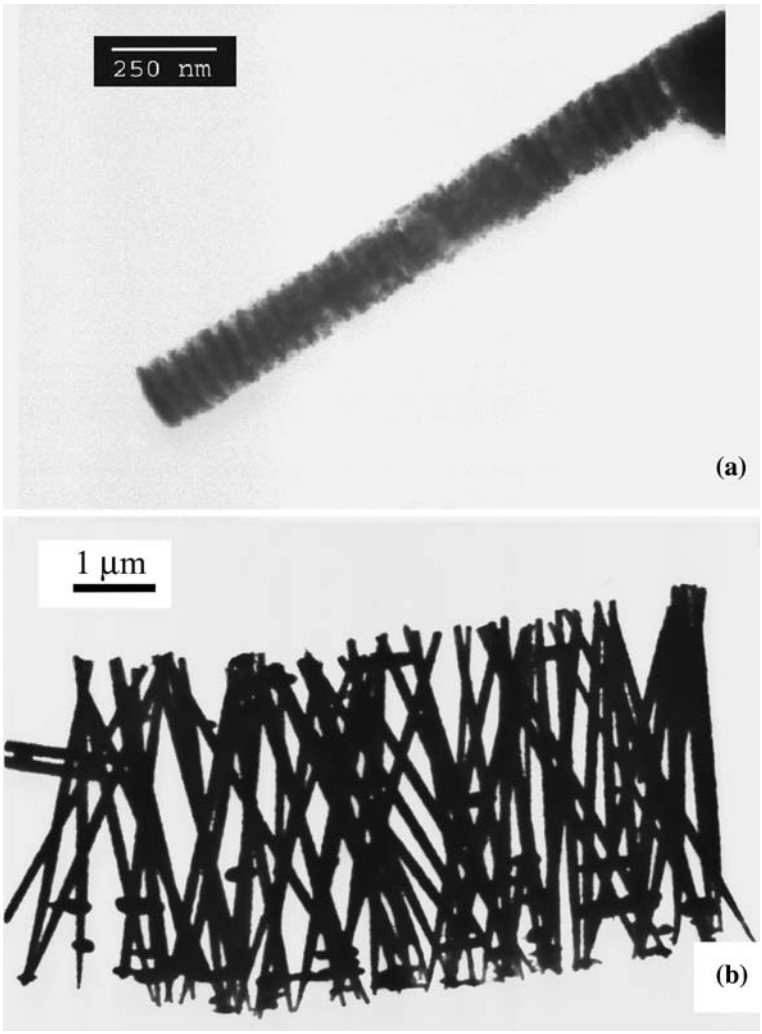

Fig. 1. TEM micrographs of nanowires plated in a polycarbonate membrane from Bath A: (a) 30 nm layers pulsed plated at −0.5 V for 100 s, and −1.9 V for 8 s, (b) lower magnification micrograph showing the wire lengths.

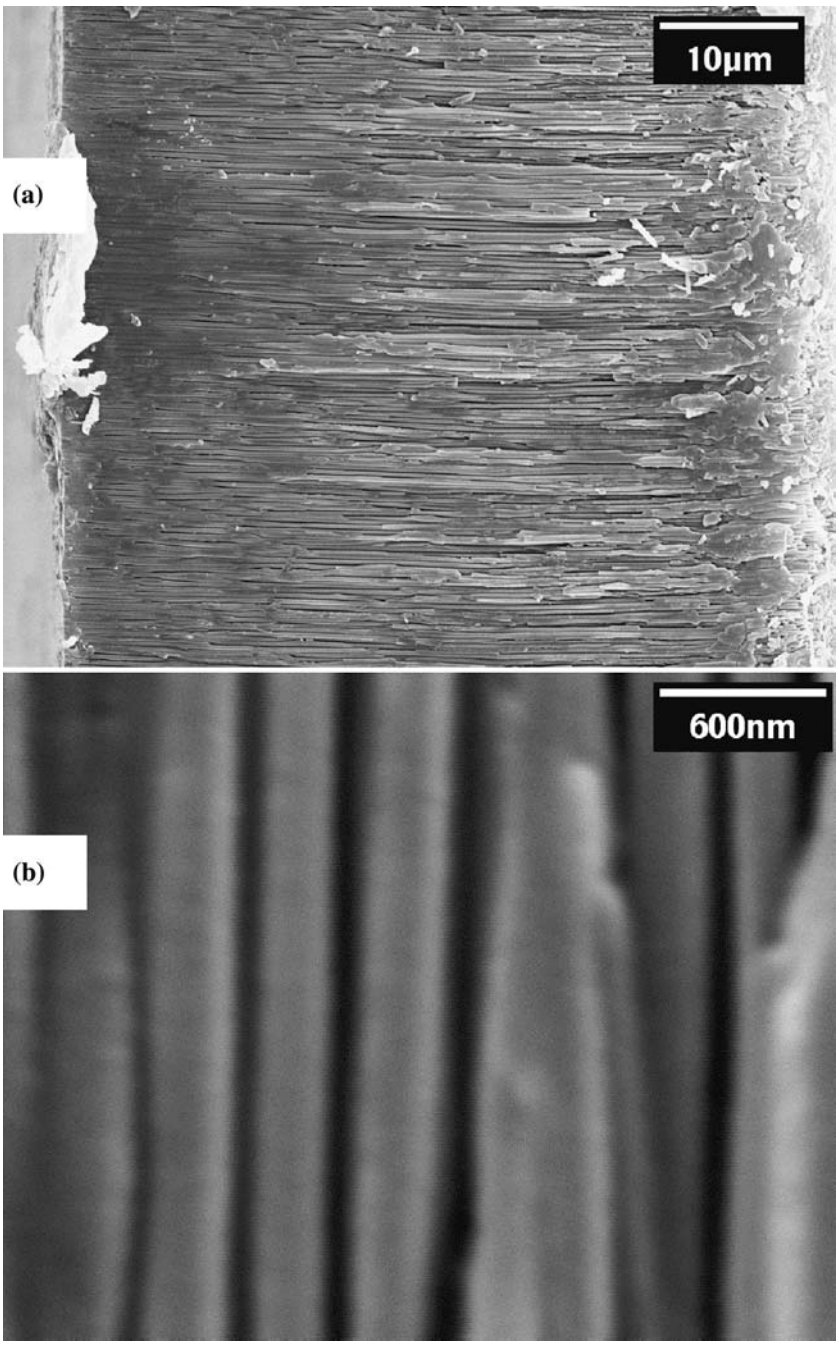

Fig. 2. Cross-sectional SEM image of AAO membrane at (a) low and (b) high magnifications.

and the potential was corrected for the ohmic drop, measured by impedance analysis, with a BAS-ZAHNER IM6 impedance measurement unit. Deposit composition was analyzed with a KEVEX Omicron energy dispersive X-ray fluorescence analyzer (XRF). Current efficiency was obtained with anodic stripping in 0.2 M HCl solution [40–41].

AAO (Whatman Anodisc®) and polycarbonate (Whatman Nuclepore®) membranes were used as templates for nanowire plating. The stated pore size of the AAO membranes by the manufacturer was 20 nm, and that for polycarbonate membranes was 50 nm. A layer of Au was sputtered on one side of the membranes to serve as a conducting substrate and to seal the nanometric pores. The membranes were fixed on a stationary holder for plating, with an exposed area of 2.25 cm^2. No electrolyte agitation was applied. After nanowire plating, 1 M NaOH solution and dichloromethane were used to dissolve the AAO and polycarbonate membranes, respectively, to release the nanowires.

Different plating schemes were investigated. DC plating was carried out potentiostatically, with a PC-controlled Pine Instrument bi-potentiostat. Pulse plating, with either an AMEL (model 568) or Solatron (model SI 1287) function generator, was used in plating multilayers, potentiostatically or galvanostatically. In

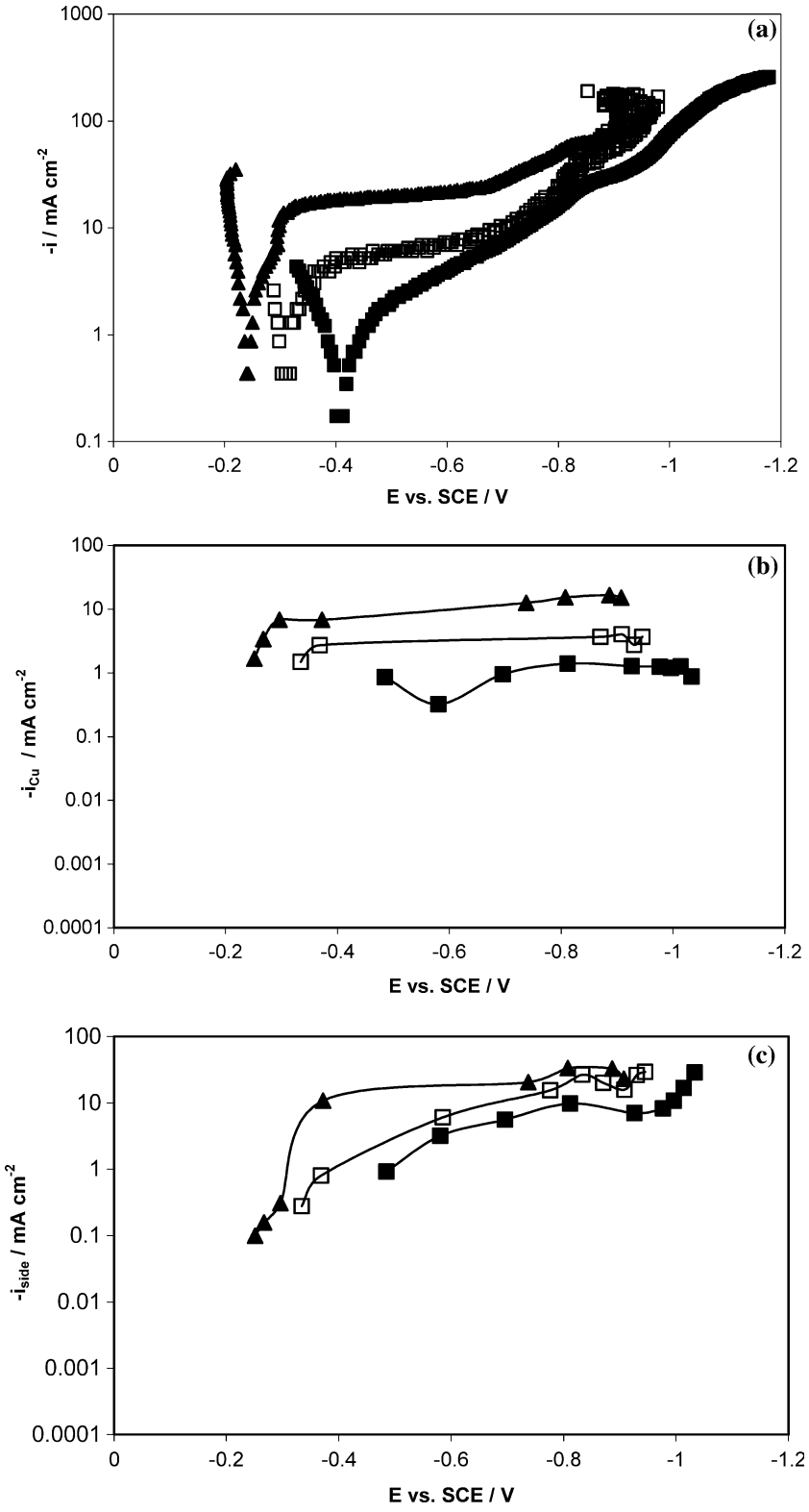

Fig. 3. Characterization of Bath B deposition ■: 0.003, □: 0.01, ▲: 0.03 M Cu(II): (a) polarization curves; (b) Cu partial current densities; (c) side reaction partial current densities; (d) deposit composition (+: Fe, ■: Co, ▲: Ni, □: Cu); and (e) current efficiency at different current densities.

general, Cu and Co-rich FeCoNiCu alloys were deposited at low and high cathodic current/potential, respectively, at different times. In a triple galvanostatic pulse scheme, a zero current period was introduced to overcome the depletion of Cu cation and local pH rise.

A JEOL JSM-840 scanning electron microscope (SEM), was used to inspect the nanowires. Qualitative composition analysis was obtained with an energy dispersive X-ray (EDX) detector option on the SEM. Wavelength dispersive X-ray spectroscopy (WDS) was

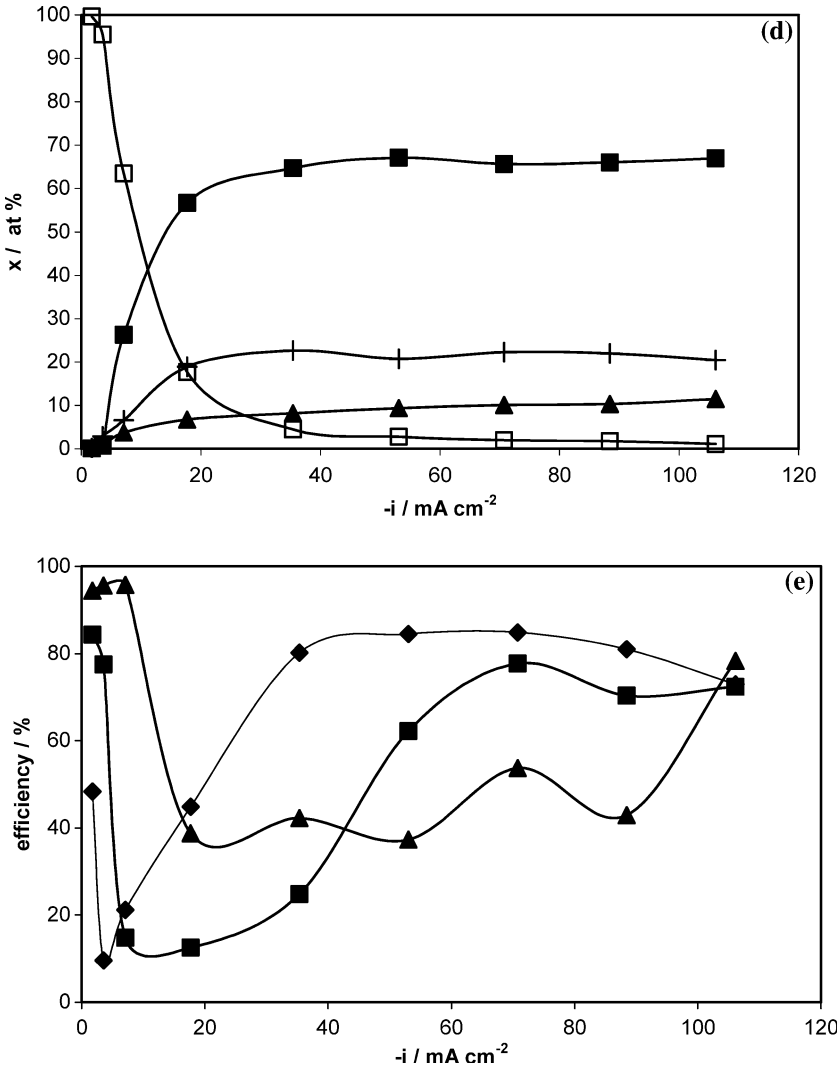

Fig. 3. Continued.

used for quantitative analysis. Detailed structure of the wire was examined with a JEOL JEM-2010 transmitted electron microscope (TEM) operated at 200 keV with a point-to-point resolution of 2.3 Å. Some TEM micrographs were obtained with a lower resolution JEM-100CX operated at 80 kV.

3. Results and discussion

The dilute electrolyte, Bath A, used for FeCoNiCu/Cu multilayer thin film deposition [37], was employed for plating nanowires with polycarbonate membranes. Figure 1 shows an example of multilayered nanowires. The nanowire shown in Figure 1(a) were deposited at −0.5 V, and −1.9 V vs SCE for 100 and 8 s, respectively. The layer structure is evident in the TEM micrographs. An estimate of the layer sizes is 30 nm for each layer. The wire diameter was about 180 nm. Figure 1(b) is a TEM micrograph of nanowires at lower magnification. The wire length was 5–6 microns.

The AAO membrane was used to fabricate longer nanowires, with the concentrated electrolyte, Bath B, to compensate for the larger diffusion resistance. An AAO membrane cross-sectional structure is shown in Figure 2(a) and (b). Figure 2(a) shows that the membrane thickness was 60 μm. Figure 2(b) is a higher magnification of the membrane and shows a pore-to-pore separation of about 350 nm.

The metal deposition rates in the concentrated bath were investigated on a rotating gold disk electrode, at 1000 rpm. Figure 3(a) presents the polarization curves for three baths with different Cu^{2+} concentrations. As expected, the open circuit potential becomes more positive as the Cu concentration increases. In the case of the solution with highest Cu, a plateau was observed at a potential between −0.3 and −0.6 V, corresponding to the Cu deposition limiting current. In the electrolyte with 0.003 M Cu(II), the limiting current density plateau was not observed in the corresponding polarization curve. The Cu limiting current was verified by the determination of the Cu partial current density in Figure 3(b), which increases proportionally with the Cu concentration in the bath. Figure 3(c) shows the partial current densities of side reactions. Comparing Figure 3(b) and (c) shows that the side reaction becomes

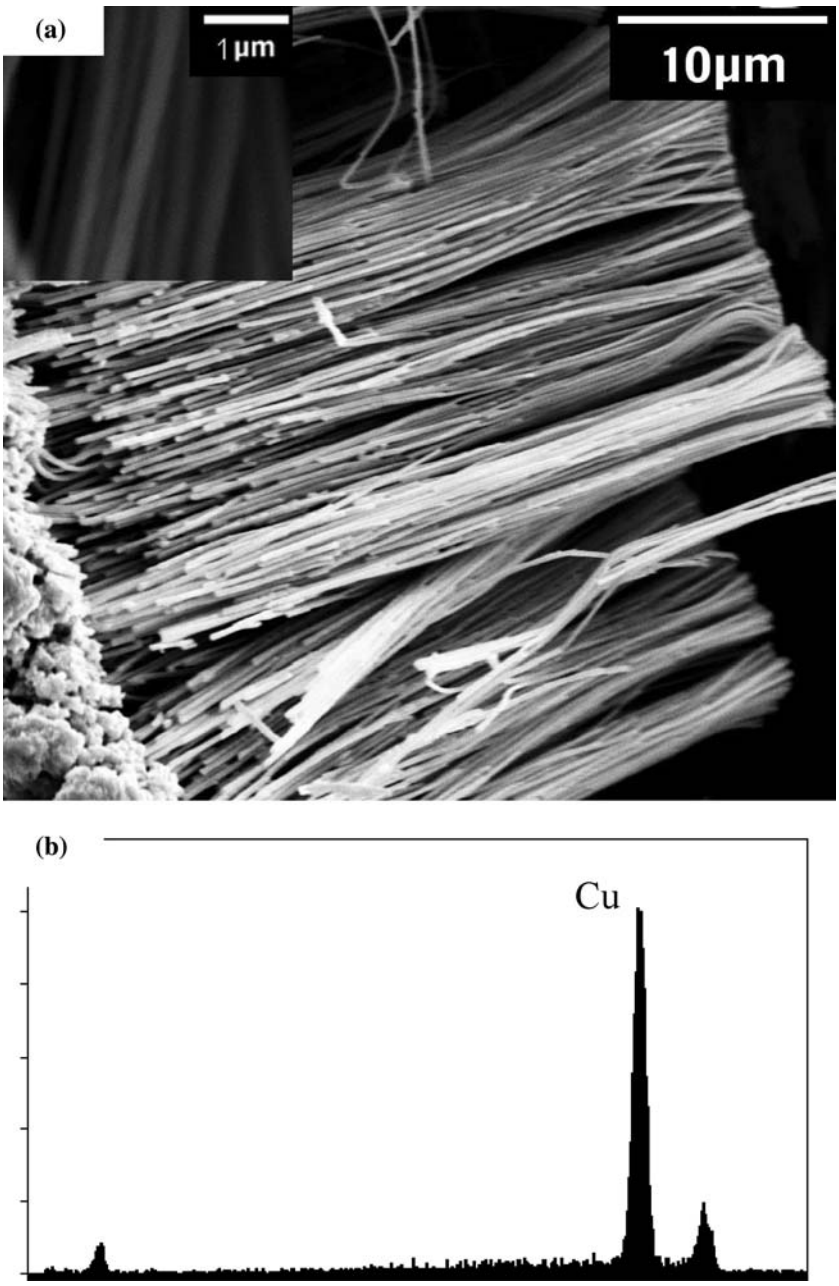

Fig. 4. (a) SEM micrograph and (b) EDX spectrum of the nanowires DC plated with AAO in Bath B, with 0.03 M Cu(II), at −0.3 V vs SCE.

higher than the Cu reduction at potentials more negative than −0.35 V vs SCE, which also explains the absence of the limiting current plateau in the total polarization curve, Figure 3(a), for the 0.003 M Cu(II) electrolyte. The deposit composition varies with the applied current density. A representative example is shown in Figure 3(d). As expected, the Cu content decreases as the applied current increases, allowing the fabrication of the multilayer structure with a pulse scheme. Figure 3(e) presents the current efficiency at different current densities. While the efficiency in Bath B with different Cu(II) concentrations have the same pattern, a higher current efficiency was observed at low current, with a value over 90% for the most concentrated Cu(II) electrolyte. As current increases, the efficiency drops as the side reaction increases. After the efficiency reaches a minimum value, it increases again due to the deposition of iron-group metals.

Figure 4(a) and (b) shows the SEM micrograph and EDX spectrum of an array of nanowires plated at a DC potential of −0.3 V vs SCE in Bath B with 0.03 M Cu(II), with the membrane removed. The nanowires were grown to a length of 35 μm. The wire diameter was consistent with pore size observed in Figure 3, 200 nm. The EDX spectrum shows that the wire was pure Cu.

Figure 5 is the current response during the DC potential plating of the wire shown in Figure 4. A current transient was observed. The lowest current, −0.6 mA, corresponds to the limiting current when the pore is empty. After the start of deposition, the current

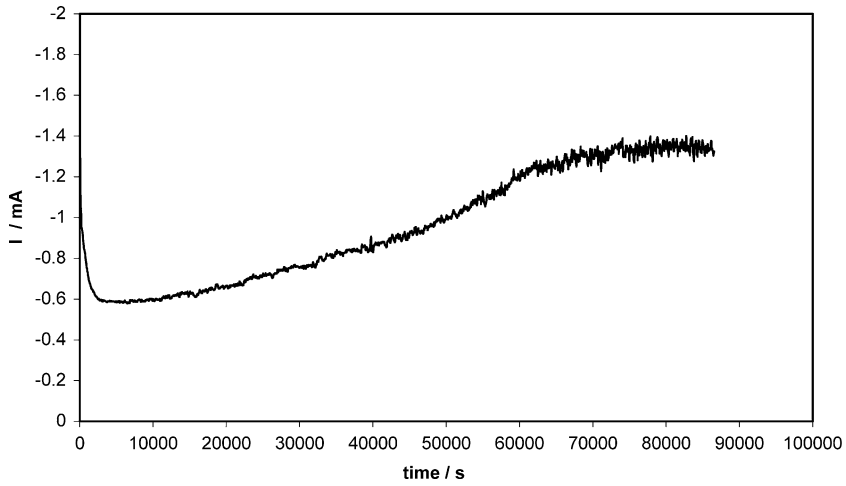

Fig. 5. Current response of nanowire plating with AAO in Bath B, with 0.03 M Cu(II), at −0.3 V vs SCE.

increases gradually during the whole plating period due to the decrease in the Cu and proton boundary layer thickness. A steady state current value was reached after 60,000 s, which corresponds to the filling of the pores.

Cu nanowires plated at a higher potential of −0.5 V vs SCE, for the same deposition time as the −0.3 V case, 60,000 s, were found to be much shorter without an overplated cap, indicating a significant side reaction effect, consistent with the partial currents shown in Figure 3(c). Unlike thin film plating, the nanometric size of the recess structure exaggerates the problem caused by side reactions. For example, a pH increase is expected in pores due to hydrogen evolution, which might cause the precipitation of metal hydroxide and cease the wire growth.

A higher potential was used to deposit alloy nanowires rich in iron-group elements. An SEM micrograph and the EDX spectrum of alloy nanowires is shown in Figure 6. The potential was constant at −1.0 V vs SCE in Bath B, with 0.01 M Cu(II). Deposition lasted for 2.5 h, and the nanowires were found to grow fully within the template, producing a mushroom-like cap on top. The wire length was 60 μm and the diameter, determined from the high resolution micrograph inset, was 200 nm. The EDX shows that the nanowire is a Co-rich FeCoNiCu alloy, which was confirmed by a composition of $Fe_{20.5}Co_{66.1}Ni_{8.9}Cu_{4.5}$ from WDS analysis.

Based on the above DC potential plating investigations, double potentiostatic pulse schemes were explored for making multilayer nanowires of FeCoNiCu/Cu. In potential pulses, at the beginning of the low potential pulse, the initial current jumps to an anodic value due to the low surface concentration of the metal ions resulting from the prior high potential pulse. In order to get around this problem, different low potential pulses were investigated in order to minimize the anodic current charge.

From the above investigation, pulse plating was performed in Bath B with 0.01 M Cu(II), with −1.0 V for 30 s and −0.55 V for 500 s. Although the Cu DC plating at −0.5 V was not as favorable as −0.3 V in terms of Cu nanowire growth, this higher potential value was required to minimize the anodic current at the low potential pulse. Figure 7 shows the current response and integrated charge, when the response is steady. The anodic charge was small compared with the deposition charge in the high potential pulses.

The SEM micrograph and EDX spectrum of the nanowires are shown in Figure 8. The nanowires are about 15 μm long, having a diameter of 180 nm. Etching was performed with HNO_3/C_2H_5OH (volumetric ratio 1:20) solution for 3 min to increase the image contrast by selectively etching a part of the Co-rich FeCoNiCu alloy [35]. The layer structure was observed after etching, with a bilayer thickness of 170 nm.

EDX spectrum shows a qualitatively higher average Cu content than Co-rich FeCoNiCu alloy nanowire shown in Figure 6, as expected, due to the layering. The average atomic composition of 15.7% Fe, 47.0% Co, 7.3% Ni, and 30.0% Cu was obtained with WDS analysis. Therefore, the Co-rich FeCoNiCu alloy is estimated to be about 2.7 times thicker than Cu layer. Thus, with the aforementioned bilayer thickness, the multilayer was 46 nm for the copper layer and 124 nm for the Co-rich FeCoNiCu alloy layer.

From Figure 7(b), the charge in a single high current pulse was −0.52 A s, and the charge in the following anodic current was 0.02 A s. Assuming that the plating during the high potential pulse is the same as the DC plating in Figure 4, a layer of 200 nm Co-rich FeCoNiCu alloy was expected. In comparison with the actual layer thicknesses, of 124 nm, the lower layer size suggests a drop in current efficiency during the transient plating period. The efficiency in the high potential pulse plating was 10%. The lower current efficiency is attributed to the mass transport enhancement of the proton and oxygen side side reaction rates at the start of deposition of the alloy layer.

A double galvanostatic pulse was also used to deposit the multilayer thin film with a relaxation period. A zero

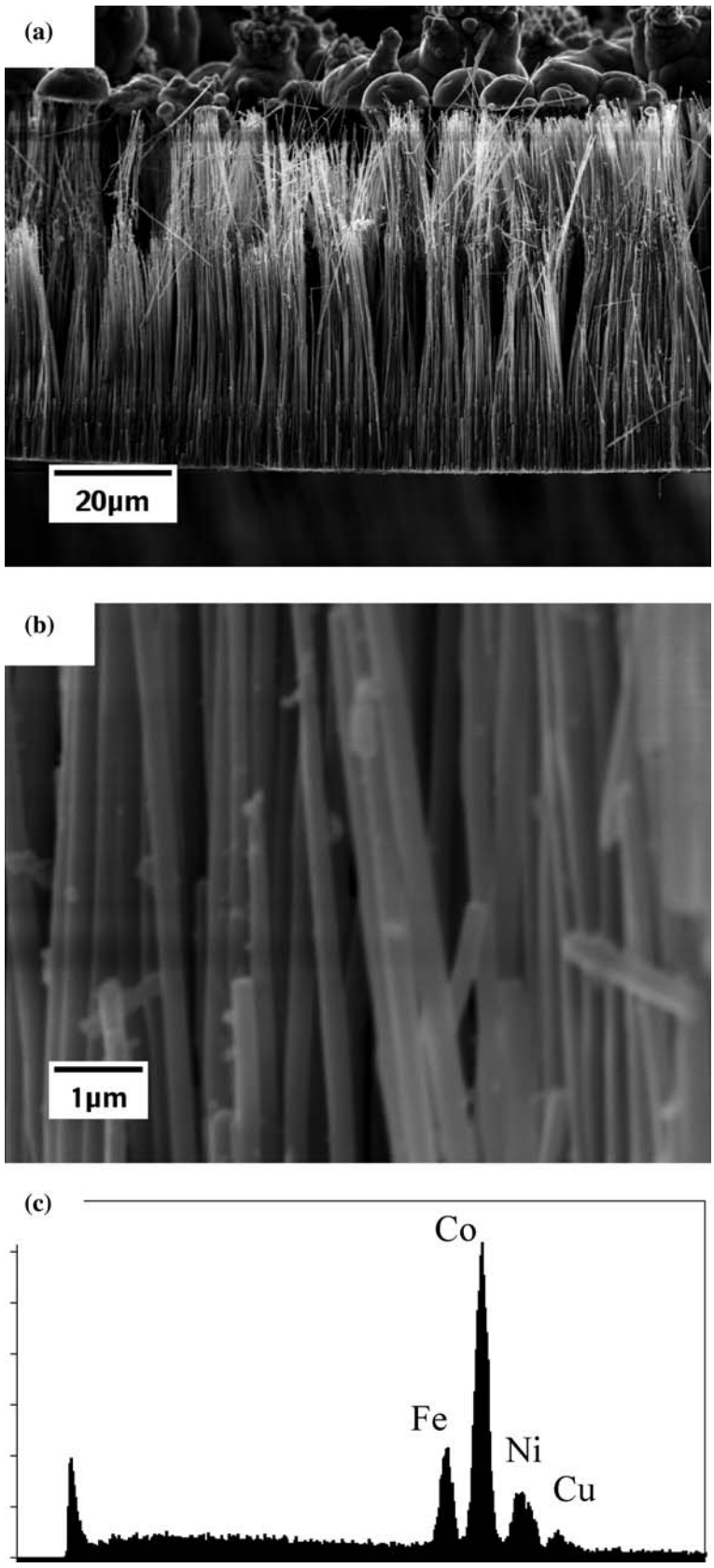

Fig. 6. Nanowires plated with AAO template in Bath B, with 0.01 M Cu(II), at −1.0 V vs SCE for 2.5 h: (a) SEM overview image; (b) enlarged micrograph; and (c) EDX spectrum.

current relaxation period was added between the high and low current pulse to allow hydrogen and hydroxide ions to diffuse out of the pores. The current for Cu layer deposition was determined from a DC potential pulse at −0.3 V vs SCE. Figure 9 is the current response of this pulse in Bath B with 0.003 M Cu(II). The current was

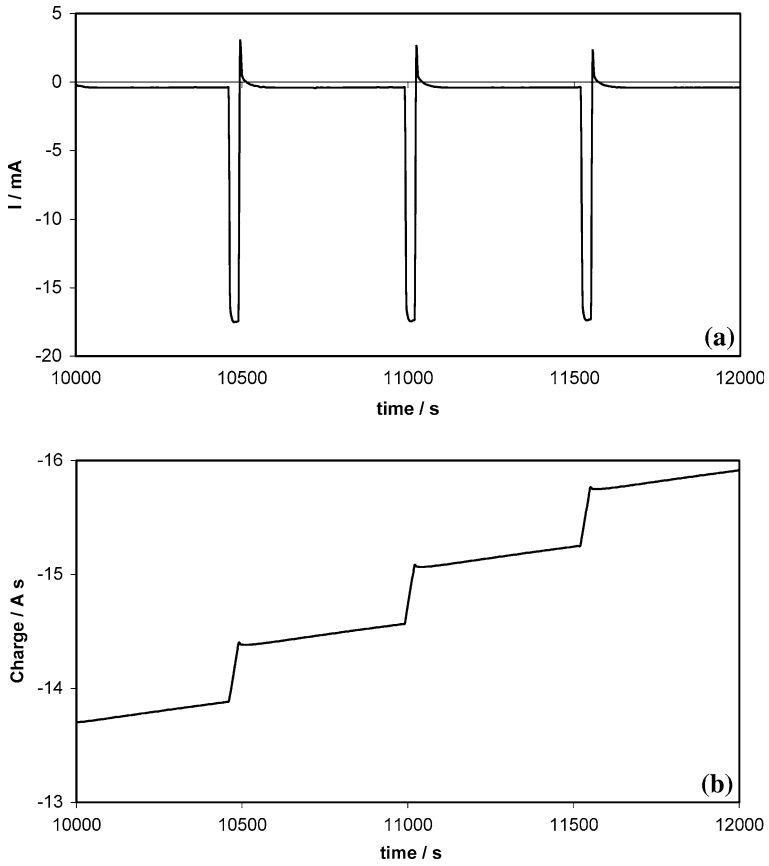

Fig. 7. (a) Current response and (b) total charge of nanowire plating with AAO in Bath B at potential −1.0, −0.55 V vs SCE for 30 and 500 s, respectively.

found to decease and approach a limiting current of $-60\,\mu$A. This minimum current is the limiting current at the bottom of the template.

A triple pulse plating was carried out at $-60\,\mu$A, −7 mA and 0 mA for 30, 0.4 and 100 s, respectively, from Bath B containing 0.003 M Cu(II). A multilayer structure was observed from TEM analysis. Figure 10(a) presents a bright field image of the nanowire. The bright layer is Cu and the dark layer is Co-rich FeCoNiCu alloy. The layer thicknesses estimated from the micrograph in Figure 10(a) are 1.8 nm Cu and 4.0 nm Co-rich alloy. The Cu thickness is consistent with a Faraday's law calculation using the current efficiency obtained with DC plating, shown in Figure 4. When controlling current, the plating charge is constant, which fixes the layer sizes. However, the limiting current densities will increase as the nanowire grows and the current efficiency changes. Thus, larger layer sizes are expected along the nanowire length if metal deposition is under transport control in competition with the kinetically controlled, water reduction side reactions.

When the pores are empty, the limiting currents of different partial reactions, for an effective area of 0.1 cm^2, are estimated as: Cu $-25\,\mu$A, H −0.1 mA, Fe −0.8 mA, Co −4.5 mA and Ni −4.5 mA. Therefore, at the lower current pulse, the current, $-60\,\mu$A, is composed mainly of Cu deposition and proton reduction. Furthermore, while the proton reduction is under kinetic control (about 35% of the limiting current), the Cu deposition is under mass transport control and an increase in Cu layer thickness along the wire growth was expected.

In the high current pulse, −7 mA, not only was Cu and proton reduction under mass transport control, but also Fe deposition was under mass transport control. Both Co and Ni reduction also approaches limiting current, and water dissociation was believed to occur at this condition. Similar to the low current pulse case, as the wire grows, the diffusion layer for all the metal species decreases and the Co-rich FeCoNiCu alloy layer thickness was also expected to increase. In other words, there is an improvement in current efficiency as the wire grows. In Figure 10(b), larger layer sizes, 2.5 nm Cu and 8.0 nm Co-rich FeCoNiCu alloy, were observed from regions of the nanowire closer to the top of the wire. GMR was recently reported [42] to be 5% in a 0.5 T magnetic field in this sample.

In both regions, the Co-rich layer thickness was found to be much smaller than the estimated value from DC plating, indicative of nonsteady state plating in the high current pulse [43–44]. This nonsteady state plating in the galvanostatic pulse method results not only in a composition gradient in the deposit, but also a decrease in current efficiency from steady state. Due to the larger diffusion distance, the transient effect is expected to be even more severe than the case in thin film plating. Furthermore, a displacement of Co-rich FeCoNiCu

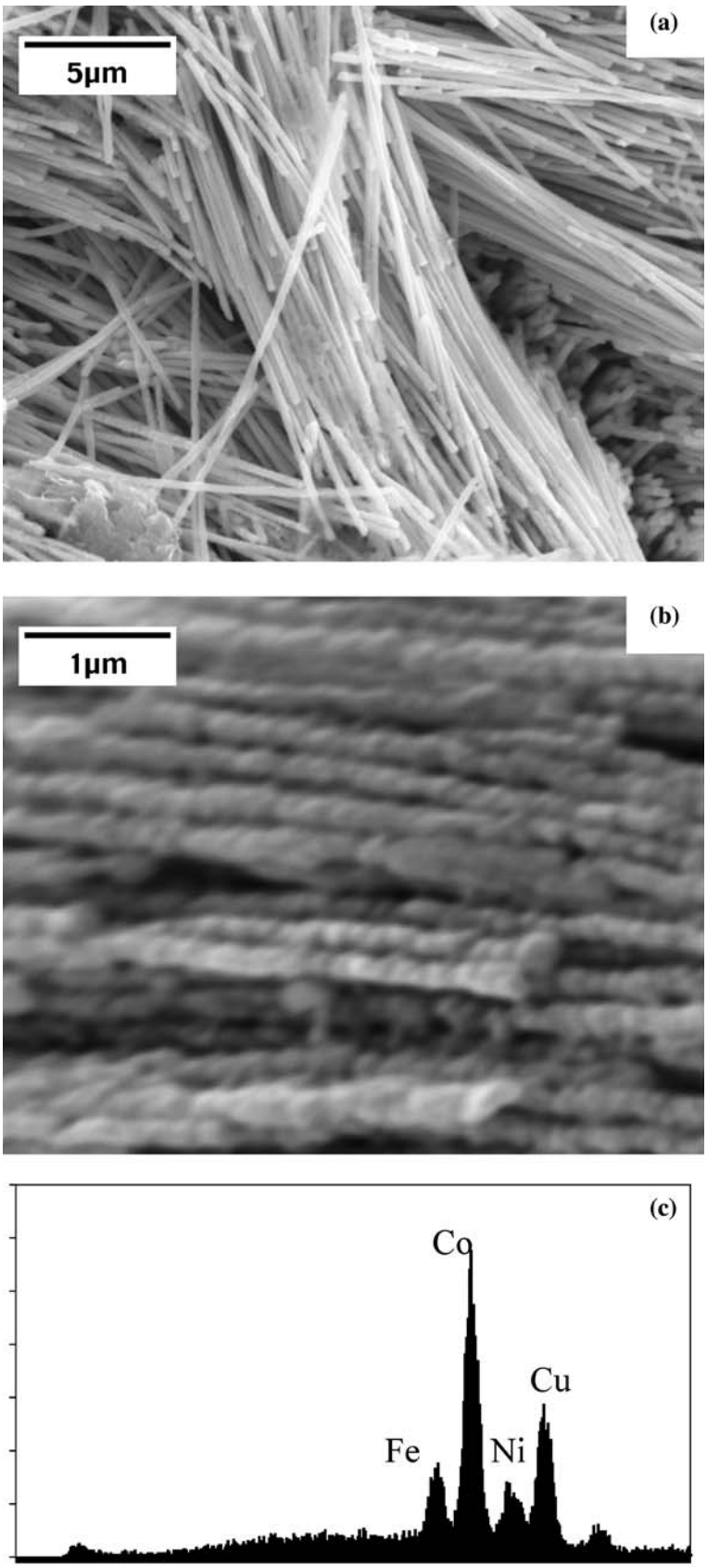

Fig. 8. SEM micrographs of nanowires plated with AAO template in Bath B, with 0.01 Cu(II), with potential −1.0, −0.55 V vs SCE for 30 and 500 s: (a) as deposit, (b) after selective etching in HNO_3/Ethanol for 3 min; and (c) EDX spectrum.

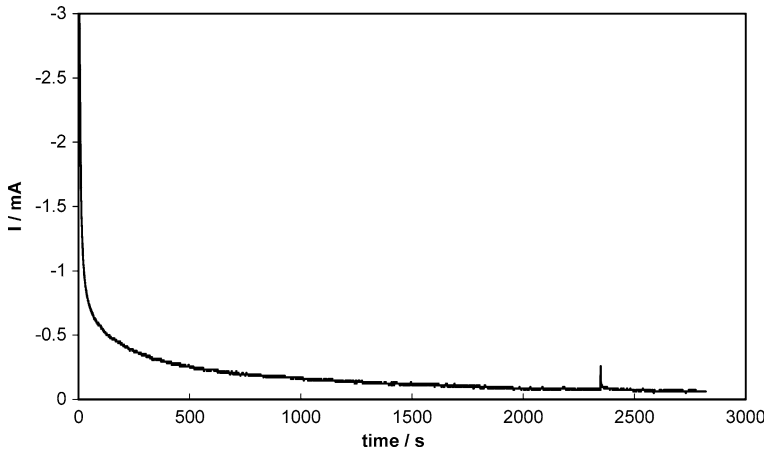

Fig. 9. Current response of a DC potential of −0.3 V vs SCE with an AAO template in Bath B with 0.003 M Cu(II).

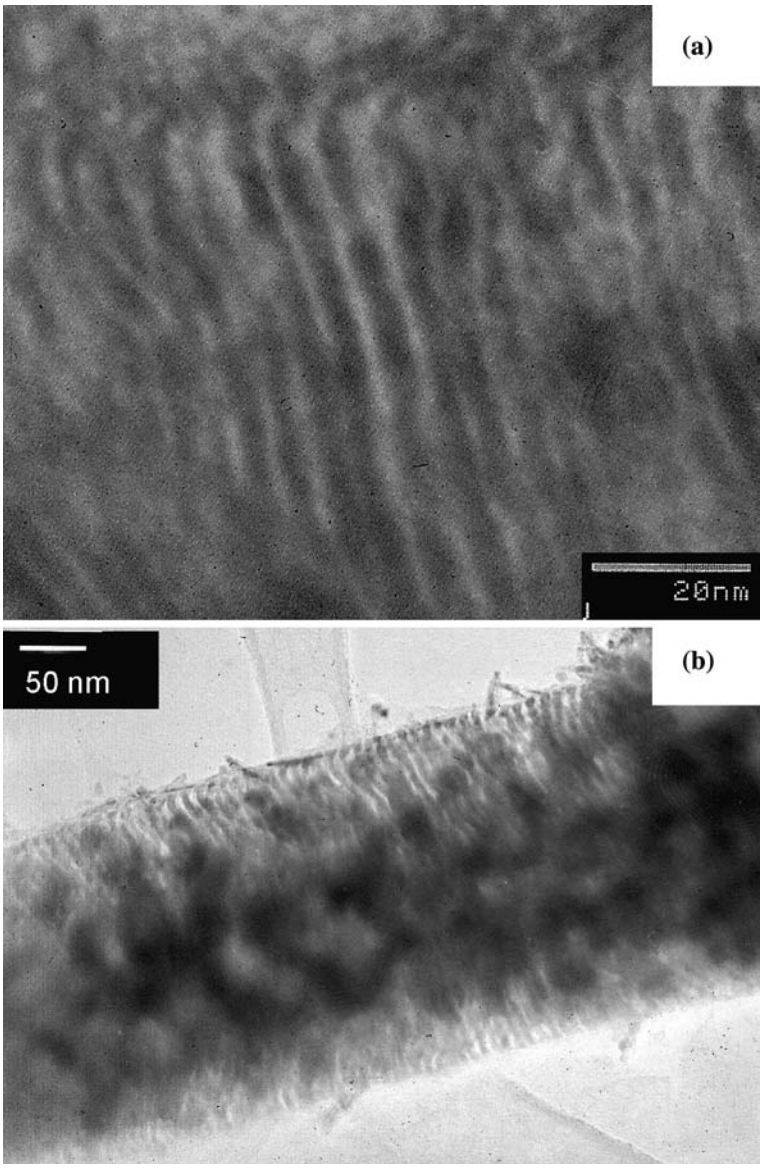

Fig. 10. TEM bright field images of two parts of nanowire plated with AAO template in Bath B, at −60 μA, −7 mA, and 0 μA for 30, 4, and 100 s, respectively.

alloy by Cu was also expected for this quaternary alloy system. Therefore, a much thinner layer thickness was expected for the Co-rich alloy layer.

4. Conclusions

A dilute electrolyte developed for multilayer thin film deposition was used successfully to fabricate nanometric multilayer nanowires in polycarbonate membranes. However, when template pores are long, a more concentrated electrolyte is more appropriate. Conditions to deposit Cu, a Co-rich FeCoNiCu alloy, and multilayered nanowires were determined. Layers of Cu and Co-rich alloys within the nanowires were clearly observed and can be controlled to below 10 nm.

Acknowledgements

This work was supported by the National Science Foundation under Grant No. CTS-0210832 and NSF-IGERT DGE-9987603.

References

1. H. Daimon and O. Kitakami, *J. Appl. Phys.* **73** (1993) 5391.
2. N. Tsuya, Y. Saito, H. Nakamura, S. Hayano, A. Furugohri, K. Ohta, Y. Wakui and T. Tokushima, *J. Magn. Magn. Mater.* **54–7** (1986) 1681.
3. D. Almawlawi, N. Coombs and M. Moskovits, *J. Appl. Phys.* **70** (1991) 4421.
4. T.M. Whitney, J.S. Jiang, P.C. Searson and C.L. Chien, *Science* **261** (1993) 1316.
5. B.J. Murray, E.C. Walter and R.M. Penner, *Nano Letters* **4** (2004) 665.
6. H.Q. Liu, J. Kameoka, D.A. Czaplewski and H.G. Craighead, *Nano Lett.* **4** (2004) 671.
7. S. Virji, J.X. Huang, R.B. Kaner and B.H. Weiller, *Nano Lett.* **4** (2004) 491.
8. J. Hahm and C.M. Lieber, *Nano Lett.* **4** (2004) 51.
9. I. Li, Y. Chen, X. Li, T.I. Kamins, K. Nauka and R.S. Williams, *Nano Lett.* **4** (2004) 245.
10. L. Piraux, S. Dubois, J.L. Duvail, K. Ounadjela and A. Fert, *J. Magn. Magn. Mater.* **175** (1997) 127.
11. S. Dubois, L. Piraux, J.M. Beuken, J.L. Duvail, A. Fert, J.M. George and J.L Maurice, *J. Magn. Magn. Mater.* **165** (1997) 30.
12. W. Schwarzacher, O.I. Kasyutich, P.R. Evans, M.G. Darbyshire, Y. Ge, V.M. Fedosyuk, F. Rousseaux, E. Cambril and D. Decanini, *J. Magn. Magn. Mater.* **198–199** (1999) 185.
13. L. Piraux, J.M. Beuken, S. Dubois, C. Marchal, L. Filipozzi, J.F. Despres, C. Leroy, E. Ferain, R. Legras, K. Ounadjela and A. Fert, *J. Magn. Magn. Mater.* **156** (1996) 317.
14. L. Piraux, S. Dubois and A. Fert, *J. Magn. Magn. Mater.* **159** (1996) L287.
15. B. Voegeli, A. Blondel, B. Doudin and J.-Ph. Ansermet, *J. Magn. Magn. Mater.* **151** (1995) 388.
16. A. Blondel, B. Doudin and J.-Ph. Ansermet, *J. Magn. Magn. Mater.* **165** (1997) 34.
17. S. Dubois, C. Marchal, J.M. Beuken, L. Piraux, J.L. Duvail, A. Fert, J.M. George and J.L. Maurice, *Appl. Phys. Lett.* **70** (1997) 396.
18. K. Liu, K. Nagodawithana, P.C. Searson and C.L. Chien, *Phys. Rev.* **B51** (1995) 7381.
19. A.P. Li, F. Muller, A. Birner, K. Nielsch and U. Gosele, *J. Appl. Phys.* **84** (1998) 6023.
20. G.D. Sulka, S. Stroobants, V. Moshchalkov, G. Borghs and J.-P. Celis, *J. Electrochem. Soc.* **149** (2002) D97.
21. E. Ferain and R. Legras, *Nucl. Instrum. Meth. Phys. Res.* **B82** (1993) 539.
22. J. Meir, B. Doudin and J.-Ph. Ansermet, *J. Appl. Phys.* **79** (1993) 6010.
23. G.P. Heydon, S.R. Hoon, A.N. Farley, S.L. Tomlinson, M.S. Valera, K. Attenborough and W. Schwarzacher, *J. Phys. D: Appl. Phys.* **30** (1997) 1083.
24. T. Thurn-Albrecht, R. Steiner, J. DeRouchey, C.M. Stafford, E. Huang, M. Bal and M. Tuominen, *Adv. Mater.* **12** (2000) 787.
25. K. Shin, K. Amanda, J.T. Goldbach, D.H. Kim, J.Y. Jho, M. Tuominen, C.J. Hawker and T.P. Russell, *Nano Lett.* **2** (2002) 933.
26. J.M. Garcia, A. Asenjo, J. Velazquez, D. Garcia, M. Vazquez, P. Aranda and E. Ruiz-Hitzky, *J. Appl. Phys.* **85** (1999) 5480.
27. J. Rivas, A.K.M. Bantu, G. Zaragoza, M.A. Blanco and M.C. Lopez-Quintela, *J. Magn. Magn. Mater.* **249** (2002) 220.
28. S.H. Ge, C. Li, X. Ma, W. Li, L. Xi and C.X. Li, *J. Appl. Phys.* **90** (2001) 509.
29. J. Verbeeck, O.I. Lebedev, G. Van Tendeloo, L. Cagnon, C. Bougerol and G. Tourillon, *J. Electrochem. Soc.* **150** (2003) 468.
30. Y. Peng, H. Zhang, S. Pan and H. Li, *J. Appl. Phys.* **87** (2000) 7405.
31. L. Sun, P.C. Searson and C.L. Chien, *Appl. Phys. Lett.* **79** (2001) 4429.
32. H. Zhu, S. Yang, G. Ni, D. Yu and Y. Du, *Scripta Materialia* **44** (2001) 2291.
33. H.R. Khan and K. Petrikowski, *Mater. Sci. Eng.* **19** (2002) 345.
34. I. Shao, R. C. Cammarata and P. C. Searson, Proceeding of 7th Symposium of Magnetic Materials, Processes and Devices, PV 2002–27 (The Electrochemical Society Proceedings Series, Pennington, NJ 2003), p. 461.
35. L. Piraux, J.M. George, J.F. Despres, C. Leroy, E. Ferain, R. Legras, K. Ounadjela and A. Fert, *Appl. Phys. Lett.* **65** (1994) 2484.
36. A. Blondel, J.P. Meier, B. Doudin and J.-Ph. Ansermet, *Appl. Phys. Lett.* **65** (1994) 3019.
37. Q. Huang, J.Y. Chan, D.P. Young, J. Jiang and E.J. Podlaha, *J. Electrochem. Soc.* **149** (2002) C349.
38. Q. Huang, D.P. Young and E.J. Podlaha, *J. Appl. Phys.* **94** (2003) 1864.
39. M. J. Madou, Fundamentals of Microfabrication: the Science of Miniaturization, 2nd edition (CRC Press, LLC 2002) p. 293.
40. P.C. Andricacos, *J. Electrochem. Soc.* **142** (1995) 1824.
41. J. Horkans, I-Chia Hsu Chang, P.C. Andricacos and E.J. Podlaha, *J. Electrochem. Soc.* **138** (1991) 411.
42. E. J. Podlaha, Y. Li, Q. Huang, J. Zhang, D. Davis, M. Guan, M. Moldovan and D. Young, "Electrodeposited GMR Multilayer Thin Films, Nanowires and Microposts," 2004 Joint International Meeting of The Electrochemical Society (ECS) and the 2004 Fall Meeting of the Electrochemical Society of Japan, Honolulu, HI, Oct. 4–8 (2004).
43. Q. Huang and E.J. Podlaha, Proceeding of 7th Symposium of Magnetic Materials, Processes and Devices, PV 2002–27 (The Electrochemical Society Proceedings Series, Pennington, NJ 2003) pp. 414.
44. Q. Huang and E.J. Podlaha, *J. Electrochem. Soc.* **151** (2004) C119.